Available online at www.sciencedirect.com
SCIENCE DIRECT®
Journal of Sound and Vibration 286 (2005) 313–339
JOURNAL OF SOUND AND VIBRATION
www.elsevier.com/locate/jsvi

A point collocation approach to modelling large dissipative silencers

R. Kirby[a,*], J.B. Lawrie[b]

[a]*School of Engineering and Design, Mechanical Engineering, Brunel University, Uxbridge, Middlesex, UB8 3PH, UK*
[b]*School of Information Systems, Computing and Mathematics, Mathematical Sciences, Brunel University, Uxbridge, Middlesex, UB8 3PH, UK*

Received 13 August 2003; received in revised form 1 September 2004; accepted 5 October 2004
Available online 18 January 2005

Abstract

A numerical matching technique known as point collocation is used to model mathematically large dissipative splitter silencers of a type commonly found in HVAC ducts. Transmission loss predictions obtained using point collocation are compared with exact analytic mode matching predictions in the absence of mean flow. Over the frequency range in which analytic mode matching predictions are available, excellent agreement with point collocation transmission loss predictions is observed for a range of large splitter silencers. The validity of using point collocation to tackle large dissipative silencers is established, as is the computational efficiency of the method and its suitability for tackling dissipative silencers of arbitrary, but axially uniform, cross-sections.

1. Introduction

Dissipative silencers are widely used to attenuate broadband noise emanating from fluid moving devices such as internal combustion engines and fans. The silencers vary considerably in size and shape according to the application, for example automotive exhaust silencers are relatively small whereas many HVAC applications require much larger silencers. The theoretical

*Corresponding author. Fax: +44 1895 256392.
E-mail address: ray.kirby@brunel.ac.uk (R. Kirby).

0022-460X/$ - see front matter © 2004 Elsevier Ltd. All rights reserved.
doi:10.1016/j.jsv.2004.10.016

analysis of relatively small automotive dissipative silencers is now well established and silencer performance is routinely quantified in terms of silencer transmission loss. Problems arise, however, in extending these methods to larger silencers and design techniques for these silencers are less well developed. The aim of this paper is to examine the feasibility of extending a numerical modelling technique, developed for relatively small silencers, to the study of much larger bulk reacting HVAC splitter silencers.

In general there are two possible approaches to modelling finite length (bulk reacting) dissipative silencers: one may analyse the problem numerically, which generally involves the use either of the finite element method [1] or the boundary element method [2]; alternatively one may approach the problem analytically, which typically involves finding roots of the governing dispersion relation and using an orthogonality relation to match the acoustic pressure and velocity fields over the inlet and outlet planes of the silencer. As a design tool, both methods have advantages and disadvantages. By adopting a generalised numerical approach, such as the finite element method suggested by Peat and Rathi [1], it is possible, in principle, to study a silencer of any shape or size. However, the number of degrees of freedom in the problem grows rapidly as silencer dimensions and excitation frequency increases and, even for a relatively small automotive silencer, the subsequent CPU expenditure quickly becomes prohibitive (see Kirby [3]). An analytic approach is arguably preferable to a numerical one and, for automotive silencers, the mode matching approach of Cummings and Chang [4], and later Glav [5], have been shown to work well, although only in the case of zero mean flow. Analytic matching of the continuity conditions over the inlet/outlet planes of the silencer does, however, demand that a sufficient number of roots to the dispersion relation have been found in order to achieve a converged solution for the problem. That is, one should obtain a transfer matrix $\mathbf{T}$ for the silencer, whose elements t_{ij} decay rapidly with increasing i, j. A well-known problem with this method is the difficulty in locating and tracking all of the (complex) roots required to achieve a fully convergent solution, and to date this problem has yet to be overcome, even for small automotive silencers. In general, the difficulty in locating sufficient roots restricts the applicability of analytic mode matching techniques, especially for much larger silencers and/or at higher frequencies.

The extension of numerical models, first developed for relatively small silencers, to the study of much larger HVAC silencers is not straightforward. Problems arise with the large increase in the degrees of freedom necessary to achieve sufficiently accurate predictions at higher frequencies, and Cummings [6] reasoned that these problems might become "intractable". Thus, current models for HVAC silencers rely on simplifying the problem in order to achieve a tractable solution. For example, Cummings and Sormaz [7], and Kakoty and Roy [8], treat the silencer as infinite in length and predict modal attenuation. Ramakrishnan and Watson [9] attempt to model a finite length silencer, after first using the finite element method to obtain roots of the governing silencer dispersion relation, but they account for the inlet/outlet planes of the silencer only by the addition of heuristic end corrections. Whilst computing the attenuation of a few propagating modes may provide a simple guide to HVAC silencer performance, most notably at low Helmholtz numbers (defined here as $2\pi f\bar{b}/c$, where f is the excitation frequency, c is the isentropic speed of sound and $\bar{b}$ is the duct width), at higher Helmholtz numbers the influence of higher order modes becomes progressively more significant and one must use an ever increasing number of modes to represent silencer performance accurately. Furthermore, modal scattering at silencer discontinuities may significantly affect silencer performance; see for example the studies by Mechel [10,11], who used analytic mode matching techniques to quantify

scattering effects over the inlet and outlet planes of a splitter silencer. Mechel concluded that scattering, especially at the inlet plane, significantly affected silencer performance. Moreover, in order to extend the analysis to higher Helmholtz numbers Mechel [10] included higher order modes in the incident sound pressure field. More recently, Cummings [6] also included higher order incident modes in an analytic investigation of a dissipative silencer. His approach involved coupling a traditional mode-matching technique with a ray-tracing model that allows relatively high Helmholtz numbers to be analysed. Both Mechel [10] and Cummings [6] do, however, treat the absorbing material as locally reacting; such an assumption greatly reduces the applicability of each technique when analysing HVAC systems since this assumes the absorbent material is either relatively "thin", when compared to the transverse duct dimensions, or has a very high flow resistivity. Both assumptions suppress axial sound propagation inside the absorbent material, which is unlikely to be the case in, for example, a typical HVAC splitter silencer.

The key to modelling a finite length, bulk reacting, HVAC splitter silencer is to adopt a computationally efficient method whilst retaining sufficient accuracy at higher Helmholtz numbers. It is, therefore, sensible first to take advantage of the fact that most HVAC silencers have an axially uniform cross-section. Accordingly, a numerical eigenvalue analysis is carried out in Section 3 of this article, for the duct/silencer cross-section; numerical mode-matching is then used to model scattering at the silencer inlet/outlet planes. Here, a numerical mode matching procedure known as point collocation is used as this fits conveniently with a numerical (finite element) solution of the governing dispersion relation. Point collocation has already been used to model relatively small dissipative silencers, for example, Astley et al. [12] applied point collocation over a single discontinuity in a rectangular duct of dimensions 0.09×0.1 m. Astley et al. report a "good measure of correspondence" between numerical predictions and experimental measurement, but their comparison is limited to a maximum Helmholtz number of 0.55. Later, Kirby [13] modelled a dissipative silencer of elliptical cross-section and used point collocation to match over two duct discontinuities. Again, comparisons were made only with experimental data, although on this occasion a maximum Helmholtz number of 3 was reached (based on the dimension of the major axis). Good agreement between prediction and experiment is reported by Kirby [13], however at higher frequencies the validity of such comparisons is questionable because of experimental error. The studies of Astley et al. [12] and Kirby [13] cover a relatively limited range of Helmholtz numbers—where only the first few least attenuated modes are likely to influence silencer performance—and crucially only compare predictions with experiment. No information is provided on how accurately point collocation enforces the matching conditions, especially under circumstances when a large number of higher orders modes are likely to influence silencer performance. Moreover, issues such as the rate of convergence of point collocation, and the optimum number, and position, of the collocation points, have yet to be investigated. A question remains, therefore, concerning the accuracy and the numerical efficiency of point collocation when studying much larger HVAC ducts. It is this issue with which this article is concerned. Accordingly, point collocation predictions are compared with exact analytic solutions (where it is proved all required roots have successfully been located) in order to investigate the accuracy of the method, but also to identify the number of degrees of freedom required to generate predictions comparable to those found analytically. This is important, not only in investigating possible numerical problems at higher frequencies, but also in determining whether point collocation is suitable for use as a general design tool.

2. Geometry and governing equations

To fully investigate the accuracy of the point collocation technique, a splitter silencer is studied in the absence of mean flow as this facilitates the derivation of a benchmark analytic solution. Note that the orthogonality relation adopted herein is known to be invalid in the presence of mean flow (the authors are unaware of an equivalent relation when mean flow is present). In principle, there is no reason why the numerical technique presented here may not be extended to include mean flow, however this is not straightforward, and we feel it is prudent first to investigate the accuracy of the method for large Helmholtz numbers, before examining more complex problems.

The model duct is shown in Fig. 1. The duct walls are rectangular in cross-section and assumed to be rigid and impervious to sound. The silencer section is located in the region $0 \leqslant \bar{x} \leqslant \bar{L}$ and consists of a bulk reacting (isotropic) porous material lining opposite walls, and a single, centrally placed, splitter of the same material. A multimode incident sound field propagates along the inlet duct towards the silencer. We choose here to restrict the incident sound field to transverse modes symmetric about the $\bar{z}$-axis only, neglecting those modes symmetric about the $\bar{y}$-axis. This allows for a simplification of the ensuing numerical and analytic analysis since only a two dimensional $(\bar{x}, \bar{y})$ representation of the problem is necessary; more importantly this assumption realises significant savings in CPU expenditure. Of course, higher order modes symmetric about the $\bar{y}$-axis will be present in a real inlet duct system, as well as in the silencer section itself, however these are neglected in the belief that their influence on the overall performance of the silencer will be relatively small (this issue is discussed further in Section 4). It should be noted, however, that the point collocation approach described here may readily be extended to study a fully three-dimensional problem.

It is convenient here to non-dimensionalise the length scales in the problem such that $x = k\bar{x}$, $y = k\bar{y}$ etc., where the "barred" quantities are dimensional and $k = \omega/c$ (ω is the radian frequency). Further, the acoustic velocity potential in the duct, $\Phi(x, y; t)$, is assumed to vary harmonically with time (t), so that $\Phi(x, y; t) = \phi(x, y)e^{i\omega t}$, $(i = \sqrt{-1})$. Then the non-dimensional, time independent velocity potential in the inlet duct, ϕ_I, satisfies

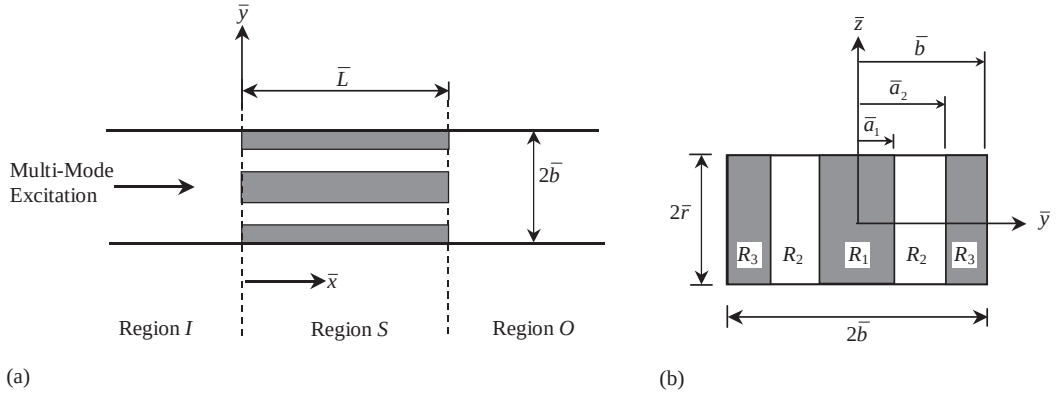

Fig. 1. (a) Plan view of silencer. (b) Silencer cross-section.

$$\left(\frac{\partial^2}{\partial x^2}+\frac{\partial^2}{\partial y^2}+1\right)\phi_I(x,y)=0, \quad -\infty<x\leqslant 0;\ 0\leqslant y\leqslant b. \tag{1}$$

Likewise, the velocity potential for the outlet duct, ϕ_O, satisfies

$$\left(\frac{\partial^2}{\partial x^2}+\frac{\partial^2}{\partial y^2}+1\right)\phi_O(x,y)=0, \quad L\leqslant x<\infty;\ 0\leqslant y\leqslant b. \tag{2}$$

For the silencer section, the velocity potential ϕ_S is expressed in terms of ϕ_I, ϕ_2 and ϕ_3, such that

$$\phi_S(x,y)=\begin{cases}\phi_1(x,y), & 0\leqslant y<a_1,\\ \phi_2(x,y), & a_1\leqslant y<a_2,\\ \phi_3(x,y), & a_2\leqslant y\leqslant b.\end{cases} \tag{3}$$

Hence,

$$\left(\frac{\partial^2}{\partial x^2}+\frac{\partial^2}{\partial y^2}-\Gamma^2\right)\phi_1(x,y)=0, \quad 0\leqslant x\leqslant L;\ 0\leqslant y<a_1, \tag{4}$$

$$\left(\frac{\partial^2}{\partial x^2}+\frac{\partial^2}{\partial y^2}+1\right)\phi_2(x,y)=0, \quad 0\leqslant x\leqslant L;\ a_1\leqslant y<a_2, \tag{5}$$

$$\left(\frac{\partial^2}{\partial x^2}+\frac{\partial^2}{\partial y^2}-\Gamma^2\right)\phi_3(x,y)=0, \quad 0\leqslant x\leqslant L;\ a_2\leqslant y\leqslant b, \tag{6}$$

where Γ is the (dimensionless) propagation constant for the porous material (assuming $\phi\propto \mathrm{e}^{-\Gamma x}$ in the material). Note that the fluid pressure and normal velocity are continuous at interfaces $y=a_1$ and $y=a_2$, for $0\leqslant x\leqslant L$, see Eqs. (16) and (17). The acoustic field in each section (the inlet, splitter and outlet section) is expanded as an infinite sum over the eigenmodes, giving

$$\phi_I(x,y)=\sum_{j=0}^{n_I}F_jZ_j(y)\mathrm{e}^{-\eta_j x}+\sum_{j=0}^{\infty}A_jZ_j(y)\mathrm{e}^{\eta_j x}, \tag{7}$$

$$\phi_S(x,y)=\sum_{m=0}^{\infty}B_m\,Y_m(y)\mathrm{e}^{-s_m x}+\sum_{m=0}^{\infty}C_m\,Y_m(y)\mathrm{e}^{s_m x}, \tag{8}$$

$$\phi_O(x,y)=\sum_{n=0}^{\infty}D_nZ_n(y)\mathrm{e}^{-\eta_n x}, \tag{9}$$

where $Y_m(y)$ is conveniently expressed as

$$Y_m(y)=\begin{cases}Y_{1m}(y), & 0\leqslant y<a_1,\\ Y_{2m}(y), & a_1\leqslant y<a_2,\\ Y_{3m}(y), & a_2\leqslant y\leqslant b.\end{cases} \tag{10}$$

Here, A_j, B_m, C_m, D_n and F_j are modal amplitudes, s_m is the wavenumber in the splitter section, $n_I + 1$ is the number of "cut-on" modes in the inlet duct and η_n is the wavenumber in the inlet/outlet section. Note that the wavenumbers s_n, $\mathrm{Re}(s_n) > 0$, $n = 0, 1, 2, \ldots$, are numbered by increasing real part. Thus s_0 is the least attenuated mode. The quantities $Z(y)$ and $Y(y)$ are the transverse duct eigenfunctions in the inlet/outlet region and the splitter section, respectively. The outlet section is assumed to be terminated anechoically.

2.1. Matching conditions

At the inlet and outlet planes of the silencer, continuity of acoustic pressure and axial particle velocity are enforced, therefore at $x = 0$ continuity of pressure yields

$$\phi_I(0, y) = \begin{cases} \beta\phi_1(0, y), & 0 \leqslant y < a_1, \\ \phi_2(0, y), & a_1 \leqslant y < a_2, \\ \beta\phi_3(0, y), & a_2 \leqslant y \leqslant b, \end{cases} \tag{11}$$

where β is the normalised complex density of the porous material ($\beta = \rho(\omega)/\rho; \rho(\omega)$ is the equivalent complex density of the porous material, see Allard and Champoux [14], and ρ is the density of air). Continuity of velocity yields

$$\frac{\partial\phi_I}{\partial x}(0, y) = \frac{\partial\phi_S}{\partial x}(0, y), \quad 0 \leqslant y \leqslant b. \tag{12}$$

At $x = L$, continuity of pressure yields

$$\phi_O(L, y) = \begin{cases} \beta\phi_1(L, y), & 0 \leqslant y < a_1, \\ \phi_2(L, y), & a_1 \leqslant y < a_2, \\ \beta\phi_3(L, y), & a_2 \leqslant y \leqslant b. \end{cases} \tag{13}$$

and continuity of velocity yields,

$$\frac{\partial\phi_O}{\partial x}(L, y) = \frac{\partial\phi_S}{\partial x}(L, y), \quad 0 \leqslant y \leqslant b. \tag{14}$$

Application of the above continuity conditions delivers an infinite system of equations which, after truncation and inversion, yields the modal amplitudes for each duct section. Before enforcing these conditions, the axial wavenumbers and transverse eigenfunctions, defined by Eqs. (7)–(9), must first be computed. Accordingly an eigenvalue analysis is performed for each duct section and this is reported in Sections 3 (numerical) and 4 (analytic). The analysis for the inlet/outlet sections is straightforward and is omitted. The appropriate transverse boundary and continuity conditions for the silencer section are given as

$$\frac{\partial\phi_1}{\partial y}(x, 0) = 0, \quad 0 \leqslant x \leqslant L; \; y = 0, \tag{15}$$

$$\frac{\partial\phi_1}{\partial y}(x, a_1) = \frac{\partial\phi_2}{\partial y}(x, a_1), \text{ and } \beta\phi_1(x, a_1) = \phi_2(x, a_1), \quad 0 \leqslant x \leqslant L; \; y = a_1, \tag{16}$$

$$\frac{\partial \phi_2}{\partial y}(x, a_2) = \frac{\partial \phi_3}{\partial y}(x, a_2) \text{ and } \phi_2(x, a_2) = \beta \phi_3(x, a_2), \quad 0 \leqslant x \leqslant L;\ y = a_2, \tag{17}$$

$$\frac{\partial \phi_3}{\partial y}(x, b) = 0, \quad 0 \leqslant x \leqslant L;\ y = b. \tag{18}$$

2.2. Incident sound field

The focus of this paper is on modelling sound attenuation in HVAC ducts over a wide range of Helmholtz numbers and it is highly likely that higher order modes in the inlet duct will be excited by a noise source such as a fan. Accordingly, a multimodal incident sound pressure field is specified here, although the detailed characteristics of this sound field will depend, to some extent, on the characteristics of the individual noise source present in an actual system. To proceed, one must know, a priori, the modal characteristics (in the form of the modal amplitudes F_j) of the chosen noise source, although obtaining this data for a fan presents many challenges. To overcome this problem, and to maintain the generality of the approach presented, we instead assign a simple heuristic relationship between the incident modal amplitudes, F_j, based on assumptions concerning the modal characteristics of the noise source. Mechel [10] suggests three possible assumptions: constant modal amplitude, equal modal power and equal modal energy density. Of these three possibilities, Mechel suggests that equal modal energy density is the most plausible representation of the modal characteristics typically found in an HVAC duct downstream from a fan (an assumption also adopted by Cummings [6]). Accordingly, in the analysis that follows we shall focus on predictions obtained assuming equal modal energy density (EMED) in the incident sound field. For the purposes of comparison, however, we also analyse the other two suggestions, equal modal amplitude (EMA), and equal modal power (EMP), in order to see how the differing assumptions affect predictions of silencer performance.

If the incident sound field is assumed to contain equal modal energy density, then the modal amplitude for propagating mode j, is given as [10]

$$\left|\frac{F_j}{p_0}\right|^2 = \frac{2\mathrm{i}}{\varepsilon_j \sum_{m=0}^{n_I} \eta_m}, \tag{19}$$

where $\varepsilon_j = \{2, j = 0/1, j > 0$. Here, p_0 is a reference pressure and is chosen, arbitrarily, to be equal to unity. It should be noted also that Eq. (19) is valid only for propagating incident duct modes; for evanescent modes, F_j is set equal to zero. Alternatively, equal modal amplitude yields [10],

$$\left|\frac{F_j}{p_0}\right|^2 = \left[\sum_{m=0}^{n_I} \frac{\varepsilon_m \eta_m}{2\mathrm{i}}\right]^{-1}, \tag{20}$$

and equal modal power,

$$\left|\frac{F_j}{p_0}\right|^2 = \frac{2\mathrm{i}}{(n_I + 1)\varepsilon_j \eta_j}. \tag{21}$$

The expressions above differ from those of Mechel [10] only in the suppression of higher order modes symmetric about the $\bar{y}$-axis. As stated earlier, this represents an approximation to the

actual problem, however we believe that the benefits of this assumption in terms of computational efficiency significantly outweigh the additional influence of these neglected modes on silencer performance.

3. Numerical model

3.1. Finite element eigenvalue analysis

An eigenvalue analysis is carried out here both for the splitter section and for the inlet and outlet ducts. The analysis for an unlined rectangular duct is reported elsewhere; for the splitter section the analysis follows closely the method of Astley and Cummings [15] and so only the final governing eigenequation is presented. Accordingly, the components of the transverse eigenfunction in each region of the splitter section are written, for mode m, as

$$y_1(y) = \beta Y_{1m}(y),\ y_2(y) = Y_{2m}(y),\ y_3(y) = \beta Y_{3m}(y), \tag{22a,b,c}$$

and these are discretised into finite elements in which the resulting nodes are numbered 1, $2, \ldots, n_1$, in region R_1, $n_1+1, n_1+2, \ldots, n_1+n_2$, in region R_2, $n_1+n_2+1, n_1+n_2+2, \ldots, n_1+n_2+n_3$, in region R_3, where n_1, n_2 and n_3 denote the total degrees of freedom in regions R_1, R_2, and R_3 respectively. The nodal values that make up the discretised transverse eigenfunctions, say $\tilde{y}_i$ for node i, form vectors $\mathbf{Y}_1$, $\mathbf{Y}_2$ and $\mathbf{Y}_3$, so that

$$y_1(y) = [N_1(y), N_2(y), \ldots\ldots, N_{n_1}(y)] \begin{bmatrix} \tilde{y}_1 \\ \tilde{y}_2 \\ \tilde{y}_{n_1} \end{bmatrix} = \mathbf{N}_1\mathbf{Y}_1 \quad 0 \leqslant y < a_1, \tag{23}$$

$$y_2(y) = \left[N_{n_1+1}(y), N_{n_1+2}(y), \ldots\ldots, N_{n_1+n_2}(y)\right] \begin{bmatrix} \tilde{y}_{n_1+1} \\ \tilde{y}_{n_1+2} \\ \tilde{y}_{n_1+n_2} \end{bmatrix} = \mathbf{N}_2\mathbf{Y}_2, \quad a_1 \leqslant y < a_2, \tag{24}$$

$$y_3(y) = \left[N_{n_1+n_2+1}(y), N_{n_1+n_2+2}(y), \ldots\ldots, N_{n_1+n_2+n_3}(y)\right] \begin{bmatrix} \tilde{y}_{n_1+n_2+1} \\ \tilde{y}_{n_1+n_2+2} \\ \tilde{y}_{n_1+n_2+n_3} \end{bmatrix} = \mathbf{N}_3\mathbf{Y}_3 \quad a_2 \leqslant y \leqslant b. \tag{25}$$

Here $N_K(y)$ are the global trial (or shape) functions of the finite element mesh. Three node isoparametric quadratic finite elements are used in each silencer region; for the inlet and outlet regions, elements and nodal locations identical to those chosen for the silencer section are also adopted. The trial expressions given by Eqs. (23)–(25) are substituted into the governing equations for the silencer section (Eqs. (4)–(6)) and, after application of the relevant matching conditions

(Eqs. (15)–(18)), a weak Galerkin treatment yields the following eigenequation,

$$\frac{1}{\beta}\left[\int_0^{a_1}\left(\frac{\mathrm{d}\mathbf{N}_1^{\mathrm{T}}}{\mathrm{d}y}\frac{\mathrm{d}\mathbf{N}_1}{\mathrm{d}y}-\left[s^2-\Gamma^2\right]\mathbf{N}_1^{\mathrm{T}}\mathbf{N}_1\right)\mathrm{d}y\right]\mathbf{Y}_1+\left[\int_{a_1}^{a_2}\left(\frac{\mathrm{d}\mathbf{N}_2^{\mathrm{T}}}{\mathrm{d}y}\frac{\mathrm{d}\mathbf{N}_2}{\mathrm{d}y}-\left[s^2+1\right]\mathbf{N}_2^{\mathrm{T}}\mathbf{N}_2\right)\mathrm{d}y\right]\mathbf{Y}_2$$
$$+\frac{1}{\beta}\left[\int_{a_2}^{b}\left(\frac{\mathrm{d}\mathbf{N}_3^{\mathrm{T}}}{\mathrm{d}y}\frac{\mathrm{d}\mathbf{N}_3}{\mathrm{d}y}-\left[s^2-\Gamma^2\right]\mathbf{N}_3^{\mathrm{T}}\mathbf{N}_3\right)\mathrm{d}y\right]\mathbf{Y}_3=\mathbf{0}. \tag{26}$$

It is convenient to express this eigenequation in matrix form, by defining matrices **A** and **C** according to

$$\mathbf{AY}=\frac{1}{\beta}[\mathbf{K}_1+\Gamma^2\mathbf{M}_1]\mathbf{Y}_1+[\mathbf{K}_2-\mathbf{M}_2]\mathbf{Y}_2+\frac{1}{\beta}[\mathbf{K}_3+\Gamma^2\mathbf{M}_3]\mathbf{Y}_3, \tag{27}$$

and

$$\mathbf{CY}=\frac{1}{\beta}\mathbf{M}_1\mathbf{Y}_1+\mathbf{M}_2\mathbf{Y}_2+\frac{1}{\beta}\mathbf{M}_3\mathbf{Y}_3, \tag{28}$$

where $\mathbf{Y}=[\mathbf{Y}_1\ \mathbf{Y}_2\ \mathbf{Y}_3]^{\mathrm{T}}$,

$$\mathbf{K}_1=\int_0^{a_1}\frac{\mathrm{d}\mathbf{N}_1^{\mathrm{T}}}{\mathrm{d}y}\frac{\mathrm{d}\mathbf{N}_1}{\mathrm{d}y}\mathrm{d}y,\ \mathbf{K}_2=\int_{a_1}^{a_2}\frac{\mathrm{d}\mathbf{N}_2^{\mathrm{T}}}{\mathrm{d}y}\frac{\mathrm{d}\mathbf{N}_2}{\mathrm{d}y}\mathrm{d}y,\ \mathbf{K}_3=\int_{a_2}^{b}\frac{\mathrm{d}\mathbf{N}_3^{\mathrm{T}}}{\mathrm{d}y}\frac{\mathrm{d}\mathbf{N}_3}{\mathrm{d}y}\mathrm{d}y,$$

and

$$\mathbf{M}_1=\int_0^{a_1}\mathbf{N}_1^{\mathrm{T}}\mathbf{N}_1\,\mathrm{d}y,\ \mathbf{M}_2=\int_{a_1}^{a_2}\mathbf{N}_2^{\mathrm{T}}\mathbf{N}_2\,\mathrm{d}y,\ \mathbf{M}_3=\int_{a_2}^{b}\mathbf{N}_3^{\mathrm{T}}\mathbf{N}_3\,\mathrm{d}y.$$

The governing eigenequation may now be written as

$$[\mathbf{A}-s^2\mathbf{C}]\mathbf{Y}=\mathbf{0}. \tag{29}$$

Eq. (29) is solved for the axial wavenumber s, and produces $n_s=n_1+n_2+n_3$ eigenvalues and associated eigenvectors. Solution of Eq. (29), and all future equations, was carried out using a FORTRAN complier and a Numerical Algorithm Group solver.

3.2. Point collocation

Point collocation demands that the acoustic pressure and particle velocity in the duct are matched at individual collocation points. The number of collocation points, n_c, is restricted to be less than or equal to the number of eigensolutions, n_s, obtained on solving Eq. (29). Accordingly, in the analysis that follows $n_c(\leqslant n_s)$ collocation points are chosen for the silencer section, and these are numbered $1,2,\ldots,r_1$, in region R_1, r_1+1, $r_1+2,\ldots,r_1+r_2$, in region R_2, $r_1+r_2+1,\ldots,r_1+r_2+2,\ldots r_1+r_2+r_3$, in region R_3, where r_1, r_2, and r_3 denote the number of collocation points in regions R_1, R_2, and R_3 respectively. For mode m, let the value of the transverse eigenfunction $y_K(y)$ (where $K=1,2$, or 3) at collocation point i, be $\tilde{p}_i$, then vectors $\mathbf{P}_1$, $\mathbf{P}_2$, and $\mathbf{P}_3$ may be constructed so that

$$\mathbf{P}_1=\left[\tilde{p}_1,\tilde{p}_2,\ldots..,\tilde{p}_{r_1}\right]^{\mathrm{T}},\ \mathbf{P}_2=\left[\tilde{p}_{r_1+1},\tilde{p}_{r_1+2},\ldots..,\tilde{p}_{r_1+r_2}\right]^{\mathrm{T}},\mathbf{P}_3=\left[\tilde{p}_{r_1+r_2+1},\tilde{p}_{r_1+r_2+2},\ldots..,\tilde{p}_{r_1+r_2+r_3}\right]^{\mathrm{T}}, \tag{30a,b,c}$$

and

$$\mathbf{P} = [\mathbf{P}_1 \mathbf{P}_2 \mathbf{P}_3]^{\mathrm{T}}. \tag{31}$$

Thus, for mode m, vectors $\mathbf{P}_1$, $\mathbf{P}_2$ and $\mathbf{P}_3$ contain the values of the transverse eigenfunctions $y_1(y), y_2(y)$ and $y_3(y)$ at the chosen collocation points in regions R_1, R_2, and R_3, respectively (note that if the location chosen for the collocation points is identical to that chosen for the nodes in the finite element mesh in Section 3.1, then $\mathbf{P} = \mathbf{Y}$). For the inlet and outlet ducts, collocation points identical to those in the silencer section are chosen, and so for mode j, the value of the transverse eigenfunction $Z_j(y)$ at collocation point i, is denoted by $\tilde{z}_i$, and

$$\boldsymbol{\Psi}_1 = \left[\tilde{z}_1, \tilde{z}_2, \ldots.., \tilde{z}_{r_1}\right]^{\mathrm{T}},\ \boldsymbol{\Psi}_2 = \left[\tilde{z}_{r_1+1}, \tilde{z}_{r_1+2}, \ldots.., \tilde{z}_{r_1+r_2}\right]^{\mathrm{T}},\ \boldsymbol{\Psi}_3 = \left[\tilde{z}_{r_1+r_2+1}, \tilde{z}_{r_1+r_2+2}, \ldots.., \tilde{z}_{r_1+r_2+r_3}\right]^{\mathrm{T}}, \tag{32a,b,c}$$

where

$$\boldsymbol{\Psi} = [\boldsymbol{\Psi}_1 \boldsymbol{\Psi}_2 \boldsymbol{\Psi}_3]^{\mathrm{T}}. \tag{33}$$

Matching proceeds (see Astley et al. [12]) by re-writing the transverse eigenfunctions in Eqs. (7)–(9), to include only the collocation points in each duct section, and then substituting the velocity potential for each region into the matching conditions described by Eqs. (11)–(14). Therefore at $x = 0$, continuity of pressure yields,

$$\sum_{j=0}^{n_I} F_j \boldsymbol{\Psi}_j + \sum_{j=0}^{n_c} A_j \boldsymbol{\Psi}_j = \sum_{m=0}^{n_c} B_m \mathbf{P}_m + \sum_{m=0}^{n_c} C_m \mathbf{P}_m. \tag{34}$$

Here, the modal sums are truncated at the number of collocation points $n_c (= r_1 + r_2 + r_3)$ for the incident and reflected modes in the splitter and the reflected modes in the inlet duct; n_I incident modes are included. Continuity of velocity at $x = 0$ yields

$$-\sum_{j=0}^{n_I} F_j \eta_j \boldsymbol{\Psi}_{1j} + \sum_{j=0}^{n_c} A_j \eta_j \boldsymbol{\Psi}_{1j} = -\frac{1}{\beta} \sum_{m=0}^{n_c} B_m s_m \mathbf{P}_{1m} + \frac{1}{\beta} \sum_{m=0}^{n_c} C_m s_m \mathbf{P}_{1m}, \tag{35}$$

$$-\sum_{j=0}^{n_I} F_j \eta_j \boldsymbol{\Psi}_{2j} + \sum_{j=0}^{n_c} A_j \eta_j \boldsymbol{\Psi}_{2j} = -\sum_{m=0}^{n_c} B_m s_m \mathbf{P}_{2m} + \sum_{m=0}^{n_c} C_m s_m \mathbf{P}_{2m}, \tag{36}$$

$$-\sum_{j=0}^{n_I} F_j \eta_j \boldsymbol{\Psi}_{3j} + \sum_{j=0}^{n_c} A_j \eta_j \boldsymbol{\Psi}_{3j} = -\frac{1}{\beta} \sum_{m=0}^{n_c} B_m s_m \mathbf{P}_{3m} + \frac{1}{\beta} \sum_{m=0}^{n_c} C_m s_m \mathbf{P}_{3m}, \tag{37}$$

Similarly, at $x = L$, continuity of pressure yields

$$\sum_{m=0}^{n_c} B_m \mathbf{P}_m \mathrm{e}^{-s_m L} + \sum_{m=0}^{n_c} C_m \mathbf{P}_m \mathrm{e}^{s_m L} = \sum_{n=0}^{n_c} D_n \boldsymbol{\Psi}_n, \tag{38}$$

and continuity of velocity yields,

$$-\frac{1}{\beta} \sum_{m=0}^{n_c} B_m s_m \mathbf{P}_{1m} \mathrm{e}^{-s_m L} + \frac{1}{\beta} \sum_{m=0}^{n_c} C_m s_m \mathbf{P}_{1m} \mathrm{e}^{s_m L} = -\sum_{n=0}^{n_c} D_n \eta_n \boldsymbol{\Psi}_{1n}, \tag{39}$$

$$-\sum_{m=0}^{n_c} B_m s_m \mathbf{P}_{2m} \mathrm{e}^{-s_m L} + \sum_{m=0}^{n_c} C_m s_m \mathbf{P}_{2m} \mathrm{e}^{s_m L} = -\sum_{n=0}^{n_c} D_n \eta_n \mathbf{\Psi}_{2n}, \tag{40}$$

$$-\frac{1}{\beta}\sum_{m=0}^{n_c} B_m s_m \mathbf{P}_{3m} \mathrm{e}^{-s_m L} + \frac{1}{\beta}\sum_{m=0}^{n_c} C_m s_m \mathbf{P}_{3m} \mathrm{e}^{s_m L} = -\sum_{n=0}^{n_c} D_n \eta_n \mathbf{\Psi}_{3n}, \tag{41}$$

It is convenient to re-arrange Eqs. (34)–(41), and to introduce $\tilde{C}_m = C_m \mathrm{e}^{-s_m L}$, to give

$$\sum_{j=0}^{n_c} A_j \mathbf{\Psi}_j - \sum_{m=0}^{n_c} B_m \mathbf{P}_m - \sum_{m=0}^{n_c} \tilde{C}_m \mathbf{P}_m \mathrm{e}^{-s_m L} = -\sum_{j=0}^{n_I} F_j \mathbf{\Psi}_j, \tag{42}$$

$$\sum_{j=0}^{n_c} A_j \eta_j \mathbf{\Psi}_{1j} + \frac{1}{\beta}\sum_{m=0}^{n_c} B_m s_m \mathbf{P}_{1m} - \frac{1}{\beta}\sum_{m=0}^{n_c} \tilde{C}_m s_m \mathbf{P}_{1m} \mathrm{e}^{-s_m L} = \sum_{j=0}^{n_I} F_j \eta_j \mathbf{\Psi}_{1j}, \tag{43}$$

$$\sum_{j=0}^{n_c} A_j \eta_j \mathbf{\Psi}_{2j} + \sum_{m=0}^{n_c} B_m s_m \mathbf{P}_{2m} - \sum_{m=0}^{n_c} \tilde{C}_m s_m \mathbf{P}_{2m} \mathrm{e}^{-s_m L} = \sum_{j=0}^{n_I} F_j \eta_j \mathbf{\Psi}_{2j}, \tag{44}$$

$$\sum_{j=0}^{n_c} A_j \eta_j \mathbf{\Psi}_{3j} + \frac{1}{\beta}\sum_{m=0}^{n_c} B_m s_m \mathbf{P}_{3m} - \frac{1}{\beta}\sum_{m=0}^{n_c} \tilde{C}_m s_m \mathbf{P}_{3m} \mathrm{e}^{-s_m L} = \sum_{j=0}^{n_I} F_j \eta_j \mathbf{\Psi}_{3j}, \tag{45}$$

$$\sum_{m=0}^{n_c} B_m \mathbf{P}_m \mathrm{e}^{-s_m L} + \sum_{m=0}^{n_c} \tilde{C}_m \mathbf{P}_m - \sum_{n=0}^{n_c} D_n \mathbf{\Psi}_n = 0, \tag{46}$$

$$\frac{1}{\beta}\sum_{m=0}^{n_c} B_m s_m \mathbf{P}_{1m} \mathrm{e}^{-s_m L} - \frac{1}{\beta}\sum_{m=0}^{n_c} \tilde{C}_m s_m \mathbf{P}_{1m} - \sum_{n=0}^{n_c} D_n \eta_n \mathbf{\Psi}_{1n} = 0, \tag{47}$$

$$\sum_{m=0}^{n_c} B_m s_m \mathbf{P}_{2m} \mathrm{e}^{-s_m L} - \sum_{m=0}^{n_c} \tilde{C}_m s_m \mathbf{P}_{2m} - \sum_{n=0}^{n_c} D_n \eta_n \mathbf{\Psi}_{2m} = 0, \tag{48}$$

$$\frac{1}{\beta}\sum_{m=0}^{n_c} B_m s_m \mathbf{P}_{3m} \mathrm{e}^{-s_m L} - \frac{1}{\beta}\sum_{m=0}^{n_c} \tilde{C}_m s_m \mathbf{P}_{3m} - \sum_{n=0}^{n_c} D_n \eta_n \mathbf{\Psi}_{3n} = 0. \tag{49}$$

Eqs. (42)–(49) form a complete set of $2(n_c + r_1 + r_2 + r_3)$ linear equations that enforce continuity of acoustic pressure and axial particle velocity at each collocation point over the inlet and outlet planes of the silencer. After substitution of appropriate values for the modal amplitudes, F_j, in the incident sound field (see Eqs. (19)–(21) for three alternative methods of specifying F_j), Eqs. (42)–(49) may be solved simultaneously for the $4n_c$ unknown modal amplitudes, A_j, B_m, $\tilde{C}_m$, and D_n. Note that in order to invert a square matrix the number of collocation points chosen, n_c, must be equal to the number of eigensolutions, n_s, taken from the solution to Eq. (29).

A popular method of representing overall silencer performance is to compute the silencer transmission loss since this is independent of any source or radiation impedance. Silencer transmission loss (TL) is defined as the ratio of the transmitted to incident sound powers. For all

choices of forcing considered here the incident sound power is unity, hence, in decibels:

$$\mathrm{TL} = -10\log_{10}\sum_{n=0}^{n_I}\frac{\varepsilon_n\eta_n}{2\mathrm{i}}|D_n|^2. \tag{50}$$

4. Analytic mode matching

An analytic model is presented here in order to provide exact "benchmark" predictions for comparison with the numerical method presented in Section 3. Accordingly an exact mode matching procedure is presented which utilises a well-known orthogonality relation in order to match over each axial silencer discontinuity. To begin with, the exact solution of the governing Helmholtz equation in the inlet and outlet region, together with rigid wall conditions at $y = 0$ and $y = b$, yields the following, well known, result for a propagating mode of order n:

$$\eta_n = \sqrt{\frac{n^2\pi^2}{b^2} - 1}, \quad \text{and } Z_n(y) = \cos\left(\frac{n\pi y}{b}\right). \tag{51a,b}$$

Solving the boundary value problem for the splitter section is rather more involved. The transverse eigenfunction for the splitter section is defined in Eq. (10). On using Eqs. (11)–(14) it is found that

$$Y_{1n}(y) = \cosh(\lambda_n y), \tag{52a}$$

$$Y_{2n}(y) = \lambda_n \sinh(\lambda_n a_1)\sinh[\gamma_n(y-a_1)]/\gamma_n + \beta\cosh(\lambda_n a_1)\cosh[\gamma_n(y-a_1)], \tag{52b}$$

$$Y_{3n}(y) = \frac{Y_{2n}(a_2)\cosh[\lambda_n(b-y)]}{\beta\cosh[\lambda_n(b-a_2)]}, \tag{52c}$$

with $\gamma_n = \sqrt{-1-s_n^2}$ and $\lambda_n = \sqrt{\Gamma^2 - s_n^2}$. The axial wavenumber for the splitter section, s, is given as a root of the dispersion relation $K(s) = 0$, where

$$K(s) = \tilde{z}(s) + \frac{\lambda\sinh[\lambda(b-a_2)]}{\beta\cosh[\lambda(b-a_2)]}\tilde{y}(s). \tag{53}$$

Here

$$\tilde{y}(s) = \lambda\sinh(\lambda a_1)\sinh[\gamma(a_2-a_1)]/\gamma + \beta\cosh(\lambda a_1)\cosh[\gamma(a_2-a_1)] \tag{54}$$

and

$$\tilde{z}(s) = \lambda\sinh(\lambda a_1)\cosh[\gamma(a_2-a_1)] + \beta\gamma\cosh(\lambda a_1)\sinh[\gamma(a_2-a_1)], \tag{55}$$

with $\gamma = \sqrt{-1-s^2}$ and $\lambda = \sqrt{\Gamma^2 - s^2}$, so that $y(s_n) = \gamma_n$, etc. Note also that $\tilde{y}(s_n) = Y_{2n}(a_2)$ and $\tilde{z}(s_n) = \mathrm{d}Y_{2n}/\mathrm{d}y|_{y=a_2}$.

This dispersion relation may be solved for the axial splitter wavenumber s_n, $n = 0, 1, 2\ldots$, using a root finding technique such as the Newton Raphson or secant method, although many other techniques are available. The success of the analytic mode matching scheme depends on computing accurately all required roots. This is a challenging task for complex roots and largely depends on the appropriateness of the initial guess supplied to the root finding algorithm. At low Helmholtz numbers, low frequency approximations of the dispersion relation may be adopted to

identify appropriate initial guesses, and one may also employ the Argument Principle to check that all roots in a specified region of the complex plane have been found. However, searching for roots in the complex plane is a laborious and cumbersome process especially at higher Helmholtz numbers where, to compound the issue, a larger number of roots must be found. To speed up the root finding procedure it is common to use a successfully located root to provide the initial guess at the next, say, frequency interval, and to track a root through the complex plane as the frequency is altered. This technique is adopted here, although it does not always work as often a root bifurcates in the complex plane, causing one or more roots to be missed at the next frequency interval. This phenomenon was evident in the current problem, even when adopting a frequency interval of 0.01 Hz. The problems described here militate against the use of the analytic technique over a large range of Helmholtz numbers. Nevertheless it is possible to demonstrate when all required roots for a certain range of parameters have successfully been located, and in so doing provide confidence in subsequent mode matching computations. The following integral relation (which is essentially the Argument Principle) is used,

$$\frac{1}{2\pi \mathrm{i}} \int_C \frac{\bar{K}'(s)}{\bar{K}(s)} \mathrm{d}s = N, \tag{56}$$

where $\bar{K}(s) = \cosh[\lambda(b-a_2)]\tilde{z}(s) + \lambda \sinh[\lambda(b-a_2)]\tilde{y}(s)$. Note $\bar{K}(s)$ is chosen to have no poles and $\bar{K}'(s)$ is the derivative of $\bar{K}(s)$. The contour C does not pass though any zeros or poles of $K(s)$ and the integer N represents the number of zeros interior to C. The contour C is chosen to include all the roots found numerically.

On successfully locating a sufficient number of eigenmodes (the Newton Raphson method was adopted here), analytic mode matching proceeds to match pressure and velocity over the inlet and outlet planes of the splitter silencer. To facilitate a convergent system of equations two orthogonality relations are used. The first is the usual orthogonality relation for $\{\cos(n\pi y/b)|n = 0, 1, 2, \ldots\}$ and the second, see [5], is

$$\beta \int_0^{a_1} Y_{1n} Y_{1m} \mathrm{d}y + \int_{a_1}^{a_2} Y_{2n} Y_{2m} \mathrm{d}y + \beta \int_{a_2}^{b} Y_{3n} Y_{3m} \mathrm{d}y = \delta_{mn} E_n, \tag{57}$$

where δ_{mn} is the Kronecker delta and

$$E_n = -\frac{1}{2s_n} \left.\frac{\mathrm{d}Y_{2n}}{\mathrm{d}y}\right|_{y=a_2} \left.\frac{\mathrm{d}K}{\mathrm{d}s}\right|_{s=s_n}. \tag{58}$$

Application of continuity of velocity and pressure at the silencer inlet, $x = 0$, yields

$$A_n = \frac{1}{\varepsilon_n \eta_n} \sum_{j=0}^{n_I} \varepsilon_j \eta_j F_j \delta_{jn} - \frac{2}{\varepsilon_n \eta_n b} \sum_{m=0}^{\infty} (B_m - C_m) s_m R_{nm}, \tag{59}$$

and

$$B_m + C_m = \frac{1}{E_m} \sum_{n=0}^{n_I} F_n R_{nm} + \frac{1}{E_m} \sum_{j=0}^{\infty} A_j R_{jm}, \tag{60}$$

respectively. Similarly at $x = L$, continuity of velocity and pressure are given as

$$D_n e^{-\eta_n L} = \frac{2}{\varepsilon_n \eta_n b} \sum_{m=0}^{\infty} (B_m e^{-s_m L} - C_m e^{s_m L}) s_m R_{nm}, \tag{61}$$

and

$$B_m e^{-s_m L} + C_m e^{s_m L} = \frac{1}{E_m} \sum_{j=0}^{\infty} D_j e^{-\eta_j L} R_{jm}, \tag{62}$$

respectively. The quantity R_{jm} is defined as

$$R_{jm} = \int_0^b \cos\left(\frac{j\pi y}{b}\right) Y_m(y) \mathrm{d}y = \frac{Q_j(s_m)}{\gamma^2 + (j\pi/b)^2} - \frac{P_j(s_m)}{\beta[\lambda^2 + (j\pi/b)^2]}, \tag{63}$$

where

$$\begin{aligned} P_j(s) = {} & \frac{j\pi}{b} \sin\left(\frac{j\pi a_2}{b}\right) \tilde{y}(s) - \beta \frac{j\pi}{b} \sin\left(\frac{j\pi a_1}{b}\right) \cosh(\lambda a_1) \\ & + \beta \cos\left(\frac{j\pi a_2}{b}\right) \tilde{z}(s) - \beta\lambda \cos\left(\frac{j\pi a_1}{b}\right) \sinh(\lambda a_1) \end{aligned} \tag{64}$$

and

$$\begin{aligned} Q_j(s) = {} & \frac{j\pi}{b} \sin\left(\frac{j\pi a_2}{b}\right) \tilde{y}(s) - \beta \frac{j\pi}{b} \sin\left(\frac{j\pi a_1}{b}\right) \cosh(\lambda a_1) \\ & + \cos\left(\frac{j\pi a_2}{b}\right) \tilde{z}(s) - \lambda \cos\left(\frac{j\pi a_1}{b}\right) \sinh(\lambda a_1). \end{aligned} \tag{65}$$

Note that $Q_j(\eta_j) = 0$ and $P_j(\tau_j) = \beta \cos(j\pi a_2/b) K(\tau_j)$, where $\tau_j = \sqrt{\Gamma^2 + j^2\pi^2/b^2}$. To solve the problem it is convenient to eliminate B_m and C_m from Eqs. (59)–(62). Two linear systems of equations are thereby obtained, namely

$$\chi_n = \frac{1}{\sqrt{\eta_n}} \sum_{m=0}^{n_I} \eta_m F_m \delta_{mn} - \frac{2}{\varepsilon_n b \sqrt{\eta_n}} \sum_{m=0}^{n_I} F_m \Lambda_{mn} - \frac{2}{\varepsilon_n b \sqrt{\eta_n}} \sum_{j=0}^{\infty} \chi_j \frac{\Lambda_{jn}}{\sqrt{\eta_j}}, \tag{66}$$

and

$$\psi_n = \frac{1}{\sqrt{\eta_n}} \sum_{m=0}^{n_I} \eta_m F_m \delta_{mn} - \frac{2}{\varepsilon_n b \sqrt{\eta_n}} \sum_{m=0}^{n_I} F_m \Omega_{mn} - \frac{2}{\varepsilon_n b \sqrt{\eta_n}} \sum_{j=0}^{\infty} \psi_j \frac{\Omega_{jn}}{\sqrt{\eta_j}}, \tag{67}$$

where

$$\chi_n = (A_n + D_n e^{-\eta_n L}) \sqrt{\eta_n}. \tag{68}$$

and

$$\psi_n = (A_n - D_n e^{-\eta_n L}) \sqrt{\eta_n} \tag{69}$$

Here,

$$\Lambda_{jn} = \sum_{m=0}^{\infty} \frac{s_m}{E_m} \tanh(s_m L/2) R_{jm} R_{nm}, \tag{70}$$

and

$$\Omega_{jn} = \sum_{m=0}^{\infty} \frac{s_m}{E_m} \coth(s_m L/2) R_{jm} R_{nm}. \tag{71}$$

Eqs. (66) and (67) may now be solved for χ_n and ψ_n after suitable truncation of the infinite sums, say at a number of eigenmodes equal to n_t. The modal amplitudes A_n and D_n may then be computed from Eqs. (68) and (69); the amplitudes B_n and C_n follow after substitution of A_n and D_n into either the pressure or velocity continuity conditions in Eqs. (60) and (62).

A key issue in the above procedure is the number of eigenmodes, n_t, at which the infinite sum is truncated. The sum must include enough eigenmodes to provide an accurate, converged, solution but the user must also ensure that no eigenmodes are missing prior to the point of truncation. Eq. (56) tells us if all roots have been located in a specified region of the complex plane but not, of course, where to locate a missing mode. On satisfying Eq. (56) the silencer transmission loss may be computed using Eq. (50), however at high Helmholtz numbers relevant eigenmodes are often missed due to failures in the tracking procedure; the effect of this on transmission loss predictions can be seen in the results presented in the following section.

5. Results and discussion

The principal behind point collocation is to enforce continuity of acoustic pressure and particle velocity at discrete transverse locations over an axial duct discontinuity, as opposed to matching analytically which seeks to enforce continuity conditions uniformly. Thus one cannot expect numerically matching to be as accurate as analytic matching, nevertheless, provided one chooses carefully the number and location of points at which numerical matching takes place, predictions should in theory tend towards those predictions obtained when matching analytically. Moreover, and this is true both for numerical and analytic mode matching, prior to matching one must ensure that a sufficient number of higher order axial modes have been computed accurately so that the sound pressure and velocity fields are accurately represented, especially either side of a discontinuity. A balance must therefore be struck between the number of axial eigenmodes required to represent accurately the continuity conditions at each collocation point, and the number of collocation points required to represent the transverse pressure and velocity fields. The analysis herein considers first how best to achieve this balance for a splitter silencer and then focuses on investigating how well point collocation performs for large splitter silencers.

The analysis in Sections 2–4 specifies non-dimensional length scales for the silencer geometry in order to reduce by one the number of parameters in the model. Silencer performance thus depends on four non-dimensional length scales: a_1, a_2, b and L. In addition, the material flow resistivity (σ) is required to fix the acoustic properties of the absorbent. The generalisation of theoretical predictions using these parameters is difficult without generating a large number of curves, especially as σ is a

complicated function of k. For example, Ramakrishnan and Watson [9] required 12 charts to "generalise" design curves for a duct lined on opposite walls, although extrapolation of their findings is far from straightforward. Similarly, Bies et al. [16] required 38 design charts to characterise a duct lined on opposite walls, although they added mean flow in the airway. Thus, generalising those results generated here, even for one source model, is likely to lead to a very long article and to detract from the main aims of the paper. Instead, to provide a rigorous examination of point collocation but economise on data presentation, we have chosen three large test silencers. For example, Silencer A has an overall width of 2 m, (thus $\bar{b} = 1$ m), a length of $\bar{L} = 2$ m, and material dimensions of $\bar{a}_1 = 0.25$ m, $\bar{a}_2 = 0.5$ m (see Table 1, which also contains details of the two other silencers, B and C). A fibrous bulk absorbing material is chosen and the generalised data of Delany and Bazley [17] are adopted, thus the propagation constant is given as

$$\Gamma = 0.189\,\xi^{-0.595} + \mathrm{i}(1 + 0.098\,\xi^{-0.7}), \tag{73}$$

and the normalised complex density as

$$\beta = -\left[0.189\,\xi^{-0.595} + \mathrm{i}(1 + 0.098\,\xi^{-0.7})\right]\left[0.087\,\xi^{-0.732} + \mathrm{i}(1 + 0.057\,\xi^{-0.754})\right]. \tag{74}$$

Here ξ is a non-dimensional frequency parameter given as $\xi = \rho f/\sigma$, where f is the excitation frequency. The flow resistivity for silencer A is chosen, arbitrarily, to be 8000 MKS Rayls/m. Note also that the formulae of Delany and Bazley are known to be invalid at low frequencies and so the semi-empirical correction formulae of Kirby and Cummings [18] are adopted to alleviate this inconsistency.

It is widely known that one can expect to rely on the accuracy of only approximately 20% of the eigensolutions found when carrying out a finite element eigenvalue analysis. For silencer A this effect is demonstrated in Table 2 by comparing solutions to Eq. (29) with those found on solving $K(s) = 0$, where $K(s)$ is given by Eq. (53), to obtain the wavenumber s at a frequency of 500 Hz. The finite element solution was generated using 5 isoparametric quadratic line elements, thus generating 11 degrees of freedom. It is noticeable in Table 2 that agreement between the two methods for the first 5 least attenuated modes may be considered acceptable, but as the mode order increases errors in the finite element solution begin to grow. Nevertheless the finite element model performs creditably (given that only 5 elements have been used to model a transverse dimension of 1 m), and computes approximately five eigenvalues relatively accurately, although the accuracy of the first two least attenuated modes is questionable. Of course, to achieve more accurate solutions the number of degrees of freedom in the mesh may be increased; for example, on using only 12 elements an error of 0.12% is observed for the least attenuated mode growing to an error of 1.4% for mode 9. Thus it is important to ensure that a sufficient number of degrees of freedom are included in order to compute accurately those axial higher order modes needed to

Table 1
Data for silencers

Silencer	Length $\bar{L}$ (m)	Width $2\bar{b}\,(m)$	$\bar{a}_1$	$\bar{a}_2$	Material flow resistivity σ (MKS Rayls/m)
A	2	2	0.25	0.5	8000
B	2	4	0.4	1.2	8000
C	2	4	1.25	1.5	16 000

Table 2
Comparison between numerical and analytic eigenvalues

Mode	Analytic		Finite element		Error in real part (%)
	Real	Imaginary	Real	Imaginary	
1	0.245192	1.045951	0.223072	1.055412	9.02
2	0.833424	0.593330	0.885459	0.541869	6.34
3	0.894753	1.598022	0.894820	1.597759	0.01
4	0.924533	1.504441	0.924229	1.500974	0.03
5	1.019494	1.357102	1.020888	1.341760	0.137
6	1.430482	0.923567	1.634150	0.800204	14.24
7	1.765143	0.671366	2.240622	0.519500	26.94
8	2.104025	0.611501	2.810752	0.444239	33.59
9	2.358073	0.215525	2.975040	0.162507	26.16

represent the sound pressure and velocity at each collocation point. Normally, when studying smaller silencers, up to 6 axial higher order modes are thought to play a significant role, see for example the analytic mode matching of Cummings and Chang [4]. It is likely, however, that for much larger silencers additional axial higher order modes will need to be considered.

The results presented in this section include only those higher order modes that are symmetric about the $\bar{z}$-axis. This is a simplification of the real problem, but enables a two-dimensional analytic approach to be carried out which facilitates a fast and efficient comparison with the point collocation technique (the validation of which is the underlying motivation for the work presented here). Of course, in a real HVAC duct system a fan may also generate incident duct modes that are symmetric about the $\bar{y}$-axis. Such modes can readily be accommodated by extending the eigenvalue analysis from one to two dimensions and matching numerically over the two-dimensional cross-section to give a fully three-dimensional sound pressure distribution. This does, however, incur very a large increase in CPU expenditure. For example, it would take approximately 300 times the computational expenditure to obtain three-dimensional predictions of an accuracy comparable to those obtained using a two-dimensional model (assuming a solver speed proportional to N^3, N being the degrees of freedom in the finite element mesh). Furthermore, it is questionable whether those incident modes symmetric about the $\bar{y}$-axis play a significant role in the overall performance of the silencer. Preliminary results for silencers A and C (see Table 1), obtained by implementing a three-dimensional approach, have been compared with the two-dimensional predictions (albeit for a much smaller mesh density than the two-dimensional solutions shown later). These initial findings indicate that the additional effect of those modes symmetric about the $\bar{y}$-axis is small. Such observations remain to be further substantiated, however, at least for the purposes of validating the point collocation technique, we feel it is justified at this stage to neglect those incident modes symmetric about the $\bar{y}$-axis.

As discussed above, the number and location of points over which matching takes place is crucial to the success of the point collocation method. One obvious starting point is to match at collocation points equal in number to the eigenvalues deemed "accurate" on solving the eigenvalue problem. Thus, one first solves an eigenvalue problem of order n_s, then utilises only the "accurate" eigenmodes, say n_a eigenmodes (where $n_a = 0.2n_s$), and matches over n_c collocation points, remembering that n_c

must be equal to n_a to maintain a square matrix (see Section 3.2). This approach is examined in Fig. 2, under the assumption of equal modal energy density (EMED) in the incident sound field. An analytic transmission loss prediction (taking $n_t = 32$) for silencer A is compared with the point collocation method in which 12 elements ($n_s = 25$) are generated for the eigenvalue analysis and matching takes place over 5 collocation points. Hence $n_c = n_a = 0.2n_s = 5$ (see Fig. 3 for location of collocation points). It is evident in Fig. 2 that discrepancies between the two methods are apparent, even though at least 5 accurate eigenvalues have been utilised. Thus, either too few collocation points have been

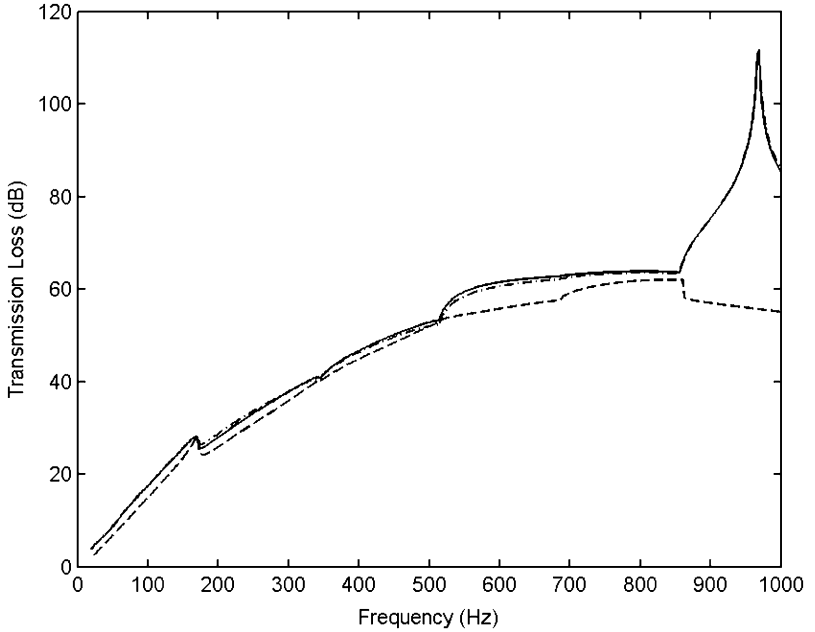

Fig. 2. Predicted transmission loss for silencer A: ———, analytic mode matching, EMED, ($n_t = 32$); – – –, point collocation, EMED, ($n_c = n_a = 5, n_s = 25$); —·—·—, point collocation, EMED, ($n_c = n_a = 25, n_s = 125$).

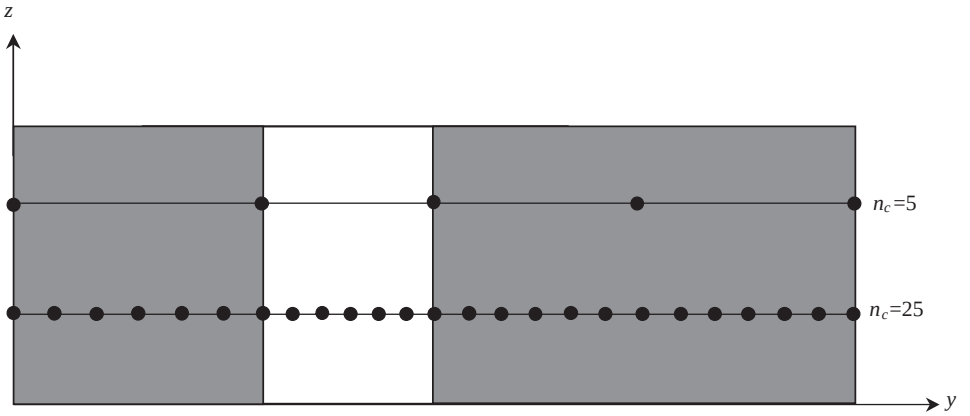

Fig. 3. Collocation points chosen for predictions shown in Fig. 2.

chosen, or too few axial higher order modes have been utilised to represent accurately the continuity conditions prior to matching. The remedy is to increase the number of collocation points, n_c, which automatically increases the number of higher order modes utilised. The effect of this is also shown in Fig. 2, where predictions are presented for $n_c = n_a = 25$, taken after solving Eq. (29) with $n_s = 125$ (see Fig. 3 for the location of the collocation points). It is evident that increasing the number of collocation points greatly increases the accuracy of the point collocation predictions, and much better agreement with the analytic solution is obtained.

The results presented in Fig. 2 suggest that for relatively large silencers, such as silencer A, a proportionately higher number of collocation points, and hence higher order modes, are required to provide an accurate solution. Although good agreement between analytic and numerical predictions is evident (for $n_c = n_a = 25$ and $n_s = 125$), point collocation is implemented only after discarding 80% of the computed eigenvalues. This may not represent a computationally efficient approach, especially if less than 25 of the computed axial higher order modes are necessary to determine accurately the pressure and velocity fields prior to matching. An alternative approach is to match numerically over collocation points coincident with the nodal locations generated in the finite element eigenvalue analysis, i.e. to set $n_c = n_a = n_s$. This approach is potentially more computationally efficient since every eigensolution is utilised, furthermore the user need only generate one set of nodal locations. Of course, one cannot expect the transmission loss predictions to be as accurate, for a given number of collocation points, since up to 80% of the eigensolutions used in matching may be inaccurate. Nevertheless, provided a sufficient number of accurate least attenuated modes are included, inaccurate higher order modes in the matching procedure should not significantly affect the collocation predictions, since their contribution to the modal sums in Eqs. (42)–(49) will be small.

In Fig. 4 point collocation and analytic transmission loss predictions are again compared for silencer A, but here the point collocation predictions were found first by using $n_c = n_a = n_s = 9$, then with $n_c = n_a = n_s = 25$ and finally with $n_c = n_a = n_s = 65$. It is evident that, as one should expect, increasing the number of collocation points improves the accuracy of the point collocation method. It is noticeable also for the case when $n_c = n_a = n_s = 25$ that the point collocation predictions are not as accurate as the equivalent predictions shown in Fig. 2, after taking $n_c = n_a = 25$ and $n_s = 125$. This is to be expected as the predictions in Fig. 4 contain many inaccurate higher order modes when compared to those in Fig. 2. Nevertheless, predictions for $n_c = n_a = n_s = 25$ compare favourably in terms of accuracy with those in Fig. 2 (except near the cut-on frequency of a higher order mode close to 1 kHz) and, if one assumes a solver of speed proportional to N^3 (for a matrix of order N), a reduction in CPU expenditure of approximately 66% is possible. As one further increases the number of degrees of freedom to $n_c = n_a = n_s = 65$, very good agreement between point collocation and analytic predictions is now possible (the two curves virtually overlap). To achieve this level of accuracy, however, requires approximately 6 times the CPU expenditure for silencer A when compared to predictions of comparable accuracy in Fig. 2, achieved after taking $n_c = n_a = 25$ and $n_s = 125$. Thus a balance must be struck between the desired accuracy of solution and computational efficiency, both in terms of solution time and operator time taken to mesh the problem. Where this balance is struck depends on the type and size of the silencer studied, and on the accuracy required. The purpose of this paper is to validate point collocation as a method applicable to large silencers, for this reason emphasis is placed here on solution accuracy rather than computational efficiency. Convergence of the finite element

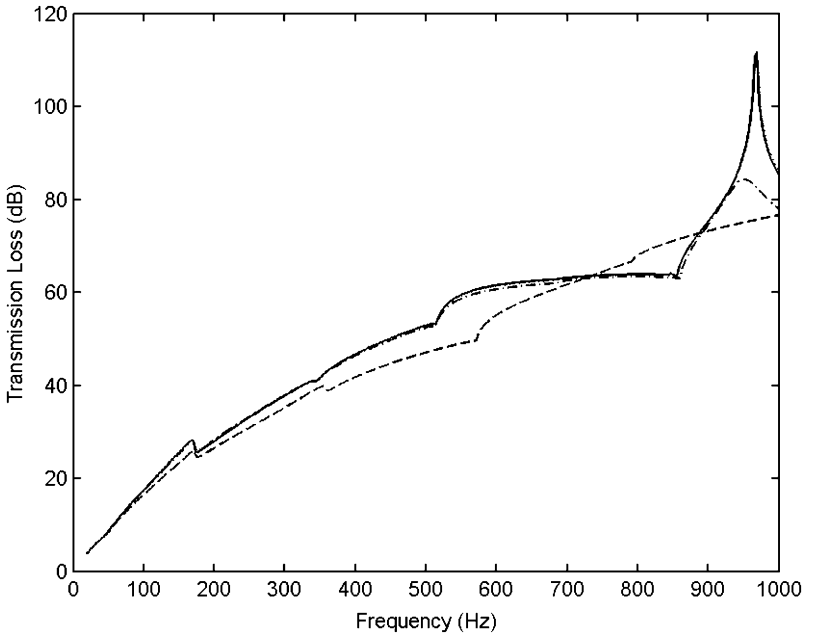

Fig. 4. Predicted transmission loss for silencer A: ———, analytic mode matching, EMED, ($n_t = 32$); – – –, point collocation, EMED, ($n_c = n_a = n_s = 9$); —·—·—, point collocation, EMED, ($n_c = n_a = n_s = 25$); - - - - -, point collocation, EMED, ($n_c = n_a = n_s = 65$), overlays analytic solution.

transmission loss predictions is therefore of utmost interest and convergence was found to be easiest to track by matching over collocation points identical to the finite element nodes generated for the eigenvalue problem; adaptation is thus carried out only for the eigenvalue mesh. The effect of systematically refining only the finite element eigenvalue mesh is demonstrated in Fig. 5, where point collocation transmission loss predictions for silencer A are compared with analytic predictions at 1 kHz (for incident EMED). Fig. 5 demonstrates systematic convergence of the point collocation predictions towards the (exact) analytic solution as the degrees of freedom are increased (taking $n_c = n_a = n_s$). This adaptation procedure may not be the most efficient computationally, but provides a safe and reliable method when studying new silencers and is therefore adopted in all further transmission loss predictions presented in this paper.

As the Helmholtz number increases, it is common practice to increase the density of the finite element mesh in order to maintain prediction accuracy. For the current method, numerical transmission loss predictions converge quickly at very low frequencies, and so, as one would expect, relatively few degrees of freedom are necessary to achieve good agreement with analytic predictions (to within 0.3 dB). At much higher frequencies, convergence is slower, however very good agreement with analytic predictions (for example, to within 0.1 dB at 4 kHz) is normally possible after a modest increase in degrees of freedom. For example, for silencer A, comparable accuracy may be achieved using 33 degrees of freedom at 100 Hz, and 65 degrees of freedom at 4 kHz: an increase in computational expenditure of approximately eight times at the higher frequency. The situation is, however, complicated by higher order incident modes, and simple linear extrapolation of the number of degrees of freedom between the two frequency extremes is

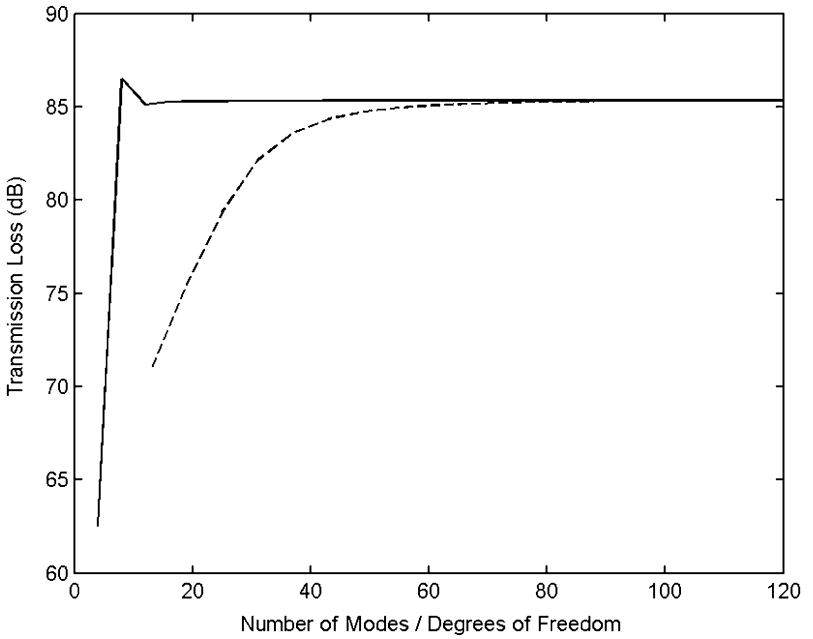

Fig. 5. Predicted transmission loss for silencer A at 1 kHz: ———, analytic mode matching, EMED ($n_t = 32$); – – –, point collocation, EMED, ($n_c = n_s$).

not possible. This is because a proportionally larger number of degrees of freedom are required close to the frequency at which the first few higher order incident modes cut-on. For example, at 1 kHz, up to 97 degrees of freedom are required to achieve agreement between numerical and analytic predictions to within 0.3 dB for silencer A. This problem does, however, disappear at higher frequencies when a large number of higher order incident modes have cut-on, since the relative proportion of incident sound power transferred to a newly cut-on mode is significantly reduced. Thus, the number of degrees of freedom required, and hence computational time, depends not only on frequency (or Helmholtz number) but also on the modal characteristics of the sound pressure field. This augurs against refining the finite element mesh solely on the basis of Helmholtz number. Instead, the mesh is refined here at the highest frequency of interest. On achieving a converged solution at this frequency (to at least 1 decimal place), the mesh density is then kept constant for calculations at every lower frequency of interest. This approach compromises computational efficiency in order to ensure an accurate solution is found over as wide a frequency range as possible, remembering that very close to the cut-on frequency of the first few incident higher order modes, it is possible some small errors may be present.

In Figs. 4 and 5 very good agreement between analytic mode matching and numerical point collocation was achieved provided enough collocation points were chosen. It is sensible to see if this observation holds for a wider range of excitation frequencies, silencer dimensions, and inlet conditions. In Fig. 6 comparisons between point collocation and analytic predictions are presented for silencer A, for frequencies up to 4 kHz and for four different incident modal conditions—EMED, EMA, EMP and plane wave (i.e. $F_0 = 1, F_1, \ldots, F_n = 0$). For each of the four different inlet conditions, excellent agreement between analytic and numerical predictions is

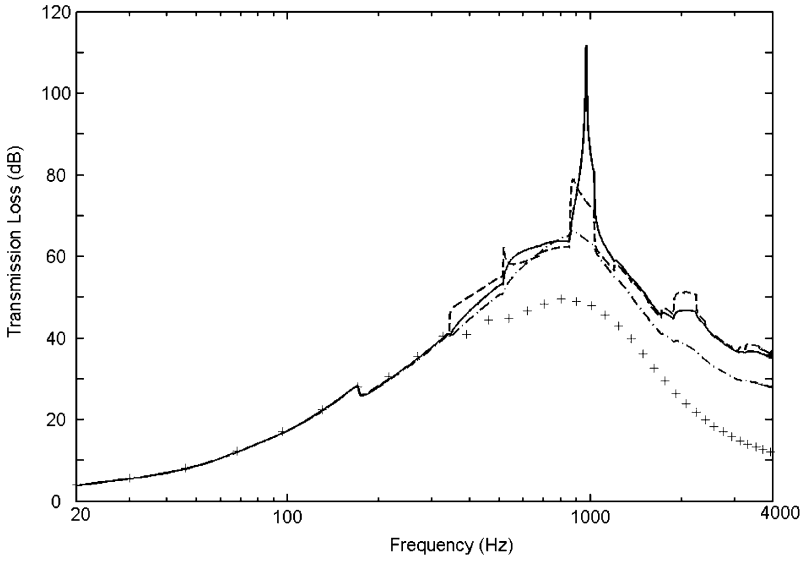

Fig. 6. Predicted transmission loss for silencer A: ———, EMED; —·——·—, EMA; – – –, EMP; +, plane wave. In each case, analytic solution ($n_t = 32$) overlays point collocation ($n_c = n_s = 65$).

evident and the two curves overlay one another. The transmission loss predictions obtained when only a plane wave is incident are, as one would expect, less than those found when the incident sound power is distributed amongst a number of higher order modes, except of course below the cut-on frequency of the first higher order mode. At the cut-on frequency of each higher order mode, sharp changes in transmission loss are clearly evident (as energy is transferred to a newly propagating mode) although as the number of cut-on modes increases this effect is progressively diluted. The three different multimode conditions adopted for the incident sound field give broadly comparable results, although the EMA predictions are consistently lower than both the EMEA and EMP predictions. It is important also to note that excellent correlation between analytic and numerical predictions has been achieved here for relatively large Helmholtz numbers (up to 73 in Fig. 6). This demonstrates the feasibility of using point collocation at higher frequencies and offers an alternative to a hybrid mode/ray model approach of the type suggested by Cummings [6].

In Fig. 7 transmission loss predictions are compared for silencer B, which has a transverse dimension double that of silencer A (see Table 1), and a different splitter width. It is evident in Fig. 7 that the agreement between the two methods is again very good, at least up to a frequency of approximately 1250 Hz. Above 1250 Hz the analytic mode matching technique fails (seen as noise in Fig. 7). This is due to one or more roots of the dispersion relation, $K(s) = 0$ (see Eq. (53)) being missed during the numerical root finding procedure. Although many of the higher order modes contribute little to the overall axial sound attenuation in the far field, they may be vital in accurately constructing the analytic pressure and velocity fields in the near field, i.e. the inlet and outlet planes. Hence these modes are required to accurately enforce the relevant matching conditions when using an analytic approach. Thus, missing even one mode may have a significant (and unpredictable) effect on the predicted sound field, see [19]

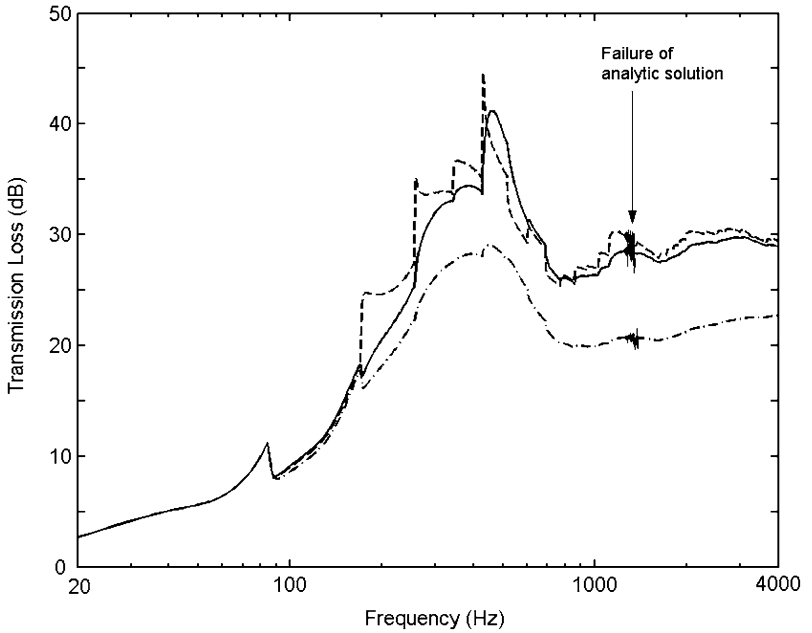

Fig. 7. Predicted transmission loss for silencer B: ———, EMED; —·—·—, EMA; – – –, EMP. In each case, analytic solution ($n_t = 64$) overlays point collocation ($n_c = n_s = 97$).

where this issue is discussed further. Moreover it is not surprising that, given the overall dimensions of silencer B, modes have been missed at frequencies above 1250 Hz. It is noticeable, however, that the analytic solution fails here at a Helmholtz number lower than that seen for silencer A, indicating that the ease of locating roots to the dispersion relation depends on the splitter geometry as well as overall duct dimensions. No such problems are apparent with the point collocation technique and stable, plausible, transmission loss predictions are evident up to a frequency of 4 kHz. Again, the EMED and EMP predictions are broadly comparable to one another, especially at higher frequencies, and the EMA predictions are consistently lower.

In Fig. 8 predictions are presented for silencer C (see Table 1) which has the same duct dimensions as silencer A, but contains a relatively narrow airway and a much higher material flow resistivity. Again the point collocation method provides predictions comparable in accuracy to analytic mode matching over the frequency range in which the analytic predictions are valid (in this case up to 350 Hz). Furthermore, for frequencies up to 4 kHz the point collocation predictions appear stable and plausible. It is noticeable that for this silencer very sharp changes in transmission loss are evident close to modal cut-on frequencies in the inlet/outlet ducts.

So far the performance of the point collocation technique has been examined solely in terms of silencer transmission loss. Although transmission loss is normally used to quantify silencer performance, it represents only a simple power balance and so may obscure detailed silencer behaviour. To compare analytic and numerical modelling techniques more closely it is useful also to analyse predictions of the axial and radial sound pressure distribution [computed directly from Eqs. (6)–(8)]. In Fig. 9 the relative axial sound pressure level is shown for the centreline ($y = 0$) of

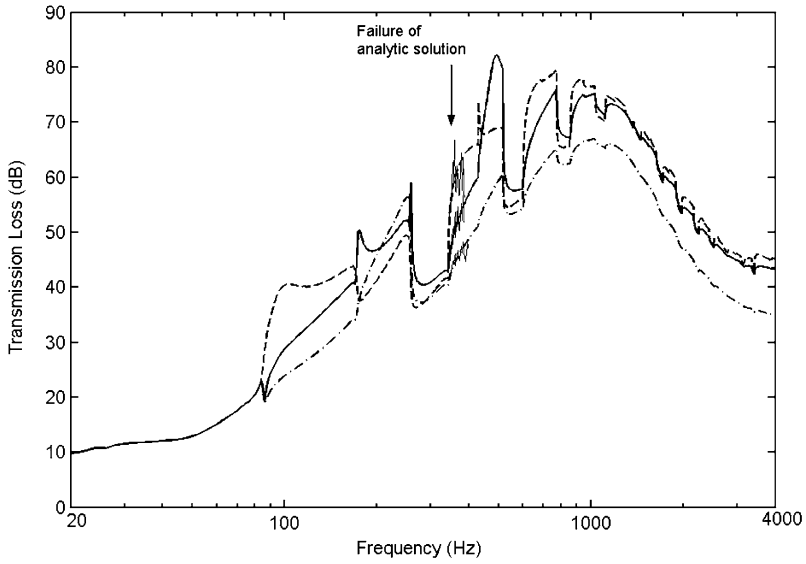

Fig. 8. Predicted transmission loss for silencer C: ———, EMED; —·—·—, EMA; – – –, EMP. In each case, analytic solution ($n_t = 64$) overlays point collocation ($n_c = n_s = 97$).

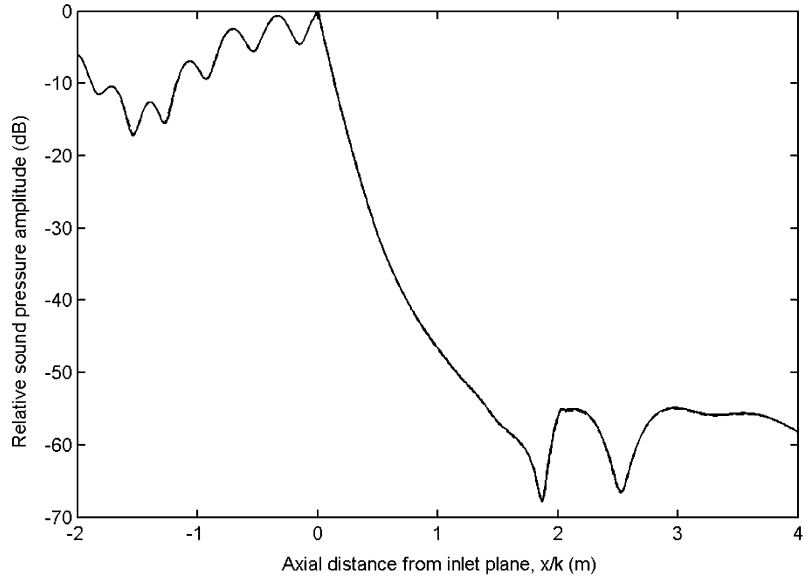

Fig. 9. Axial sound pressure level for silencer A for $y = 0$ and $f = 500$ Hz: ———, analytic mode matching, EMED, ($n_t = 64$); – – –, point collocation, EMED, ($n_c = n_s = 65$).

silencer A at a frequency of 500 Hz. Clearly, excellent agreement between point collocation and analytic mode matching is evident: the two curves overlap. Fig. 9 also demonstrates the influence of the porous material and, on the duct centre line, one may observe a reduction in sound pressure

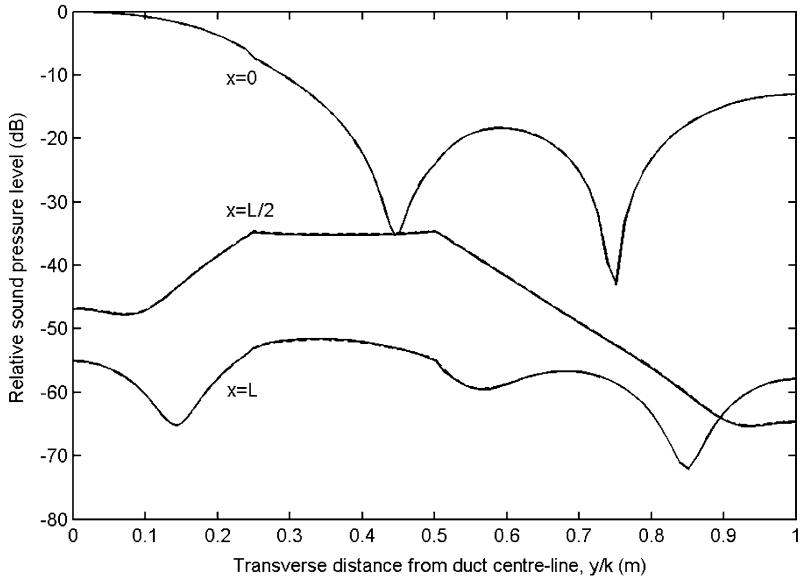

Fig. 10. Transverse sound pressure level for silencer A, at $x = 0, x = L/2$, and $x = L$, at $f = 500\,\text{Hz}$: ———, analytic mode matching, EMED, ($n_t = 64$); – – –, point collocation, EMED, ($n_c = n_s = 65$).

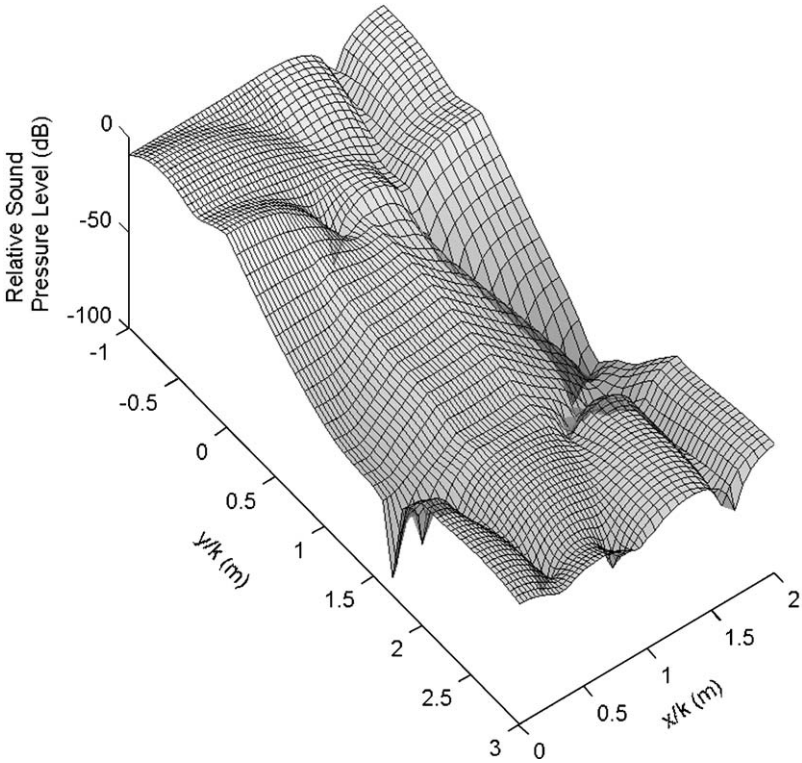

Fig. 11. Sound pressure level for silencer B, EMED, at $f = 258\,\text{Hz}$ ($n_c = n_s = 65$).

level of approximately 55 dB. In Fig. 10 the transverse sound pressure distribution is shown at axial locations of $x = 0, L/2$ and L, for silencer A at 500 Hz. Again, very good agreement between point collocation and analytic mode matching is evident, and the two sets of data overlap in a fashion similar to that seen in earlier plots. Figs. 9 and 10 demonstrate the successful implementation of the matching conditions: here analytic and numerical predictions agree to at least 3 decimal places at $x = 0$ and 1 decimal place at $x = L$. Fulfilment of the pressure gradient boundary conditions is harder to judge in Figs. 9 and 10. These conditions are also harder to enforce accurately: at $x = 0$ numerical and analytic solutions agree here to within 1 decimal place and at $x = L$ to within approximately 0.2 dB/m. This agreement can be improved by increasing the number of modes used in the analytic solution, and the number of collocation points in the numerical solution, but this will be at the cost of increased CPU time.

Finally, a three-dimensional view of the sound pressure field in silencer A is presented in Figs. 11 and 12 (constructed from point collocation predictions with $n_c = n_s = 65$). These two figures depict the sound pressure field close to modal cut-on frequencies in the inlet duct and demonstrate the complex nature of the sound field, especially close to the silencer discontinuities. Moreover, as pointed out by Mechel [11], the complex nature of the sound pressure distribution warns against field measurements where the sound pressure levels are taken only from one or two points in front of or behind the silencer.

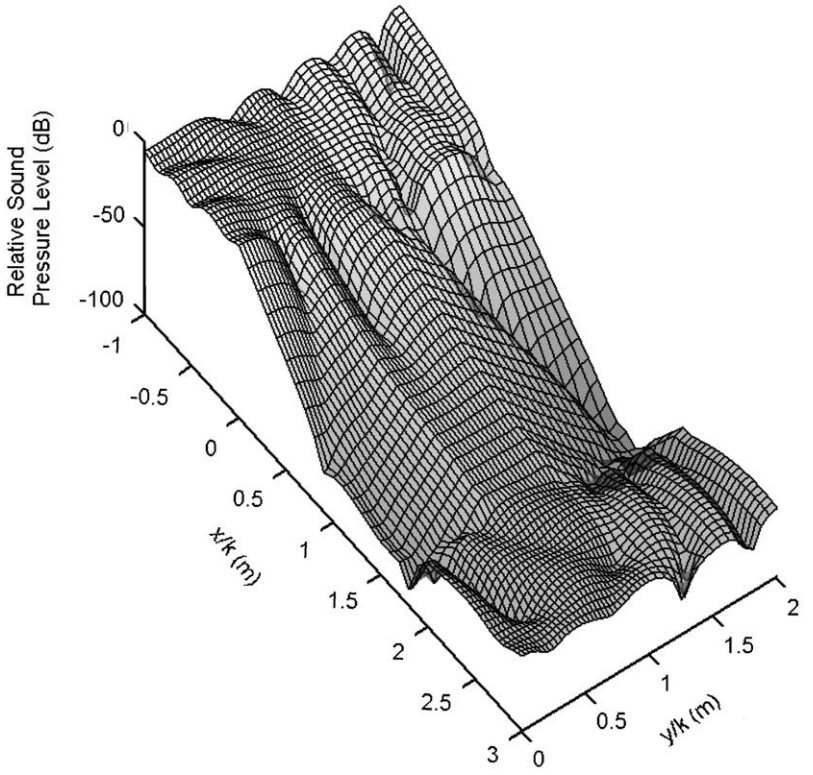

Fig. 12. Sound pressure level for silencer B, EMED, at $f = 516$ Hz ($n_c = n_s = 65$).

6. Conclusions

The efficacy of point collocation as a tool for studying large dissipative silencers has been examined here. Transmission loss predictions obtained using point collocation were compared against "benchmark" exact analytic mode matching predictions. Over the parameter range in which the exact method is valid, excellent agreement between the two methods is observed even for large dissipative silencers. It may be concluded that, provided the finite element mesh and associated collocation points are chosen using a normal adaptation procedure, point collocation offers a computationally efficient, reliable and accurate method for studying dissipative silencers in general. Although the point collocation method is restricted to axially uniform silencers, it is applicable to those of arbitrary cross-section and/or a large transverse dimension.

References

[1] K.S. Peat, K.L. Rathi, A finite element analysis of the convected acoustic wave motion in dissipative silencers, *Journal of Sound and Vibration* 184 (1995) 529–545.
[2] A.F. Seybert, R.A. Seman, M.D. Lattuca, Boundary element prediction of sound propagation in ducts containing bulk absorbing materials, *Transactions of the ASME* 120 (1998) 976–981.
[3] R. Kirby, The acoustic modelling of dissipative elements in automotive exhausts, PhD Thesis, University of Hull, 1996.
[4] A. Cummings, I.-J. Chang, Sound attenuation of a finite length dissipative flow duct silencer with internal mean flow in the absorbent, *Journal of Sound and Vibration* 127 (1988) 1–17.
[5] R. Glav, The transfer matrix for a dissipative silencer of arbitrary cross-section, *Journal of Sound and Vibration* 236 (2000) 575–594.
[6] A. Cummings, High frequency ray acoustics models for duct silencers, *Journal of Sound and Vibration* 221 (1999) 681–708.
[7] A. Cummings, N. Sormaz, Acoustic attenuation in dissipative splitter silencers containing mean fluid flow, *Journal of Sound and Vibration* 168 (1993) 209–227.
[8] S.K. Kakoty, V.K. Roy, Bulk reaction modeling of ducts with and without mean flow, *Journal of the Acoustical Society of America* 112 (2002) 75–83.
[9] R. Ramakrishnan, W.R. Watson, Design curves for rectangular splitter silencers, *Applied Acoustics* 35 (1992) 1–24.
[10] F.P. Mechel, Theory of baffle-type silencers, *Acustica* 70 (1990) 93–111.
[11] F.P. Mechel, Numerical results to the theory of baffle-type silencers, *Acustica* 72 (1990) 7–20.
[12] R.J. Astley, A. Cummings, N. Sormaz, A finite element scheme for acoustic propagation in flexible-walled ducts with bulk-reacting liners, and comparison with experiment, *Journal of Sound and Vibration* 150 (1991) 119–138.
[13] R. Kirby, Transmission loss predictions for dissipative silencers of arbitrary cross section in the presence of mean flow, *Journal of the Acoustical Society of America* 114 (2003) 200–209.
[14] J.F. Allard, Y. Champoux, New empirical equations for sound propagation in rigid frame fibrous materials, *Journal of the Acoustical Society of America* 91 (1992) 3346–3353.
[15] R.J. Astley, A. Cummings, A finite element scheme for attenuation in ducts lined with porous material: comparison with experiment, *Journal of Sound and Vibration* 116 (1987) 239–263.
[16] D.A. Bies, C.H. Hansen, G.E. Bridges, Sound attenuation in rectangular and circular cross-section ducts with flow and bulk-reacting liner, *Journal of Sound and Vibration* 146 (1991) 47–80.
[17] M.E. Delany, E.N. Bazley, Acoustical properties of fibrous materials, *Applied Acoustics* 3 (1970) 105–116.
[18] R. Kirby, A. Cummings, Prediction of the bulk acoustic properties of fibrous materials at low frequencies, *Applied Acoustics* 56 (1999) 101–125.
[19] J.B. Lawrie, R. Kirby, On analysing the performance of a dissipative silencer: a mode-matching approach, in: A.B. Movchan (Ed.), *Proceeding of IUTAM 2002/04*, Kluwer, Dordrecht